Asian Journal of Chemistry; Vol. 38, No. 8 (2026), 2005-2015
ASIAN JOURNAL OF CHEMISTRY
https://doi.org/10.14233/ajchem.2026.36269

CO_2 Desorption Characteristics of Zeolite A/X and CMS-240 under Thermal, Vacuum and CH_4 Purging Regeneration Conditions

YIHUAI HUA[1,2], XIAOJIN WEN[3,4], WEIPING ZENG[1,2], XUE ZHANG[3], QINGBO SU[1,2] and JIANFENG TANG[3,*]

[1]CNOOC Gas & Power Group, Research & Development Center, Beijing 100028, P.R. China
[2]CNOOC Key Laboratory of Liquefied Natural Gas and Low-Carbon Technology, Beijing 100028, P.R. China
[3]College of Pipeline and Civil Engineering, China University of Petroleum (East China), Qingdao 266580, P.R. China
[4]Shanghai Power Equipment Research Institute Co. Ltd., Shanghai 200240, P.R. China

*Corresponding author: E-mail: tangpaper@126.com

Received: 20 April 2026 *Accepted*: 6 June 2026 *Published online*: 7 August 2026 AJC-22426

CO_2 desorption performance is critical for adsorbent regeneration and process design in CO_2 capture systems. This work compared CO_2 desorption behaviours of 13X, 4A, 5A zeolites and CMS-240 under thermal, vacuum and CH_4 purging conditions. CMS-240 achieved excellent regeneration, with CO_2 desorption exceeding 90% under all conditions. For zeolites, pore size had a higher influence on regeneration performance than cation type. During CH_4 purging, the total purge volume primarily governed the desorption ratio. Among the tested adsorbents, 13X exhibited the highest CO_2 working capacity (3.650 mmol g^{-1}) under thermal regeneration at 200 ºC, providing valuable guidance for adsorbent selection and regeneration optimisation.

Keywords: CO_2 desorption, Adsorbent regeneration, Zeolite 13X, CMS-240, CH_4 purging, Vacuum regeneration.

INTRODUCTION

Adsorption technology has been widely applied in gas separation and purification for over 70 years and is extensively used in natural gas decarbonisation and flue gas treatment [1,2]. CO_2 adsorption technology is realised in adsorption towers, taking advantage of adsorption capacity difference of gas mixture on adsorbents, CO_2 as the component easy to be adsorbed into the porous solid material under high pressure and low temperature and hard to be adsorbed component such as CH_4 flows out of the tower. Following adsorption, CO_2 is desorbed from the adsorbent under reduced pressure and/or elevated temperature to regenerate the adsorbent. Regeneration can be accomplished using thermal, purge-gas or vacuum techniques, all of which require external energy. Consequently, adsorbent regeneration represents one of the major contributors to the energy demand of adsorption-based gas separation processes.

Although CO_2 desorption is theoretically the reverse of adsorption, the two processes are not fully reversible due to the heat effects and strong adsorbate–adsorbent interactions, resulting in incomplete CO_2 desorption from the adsorbent [3]. Therefore, regeneration characteristics are a critical indicator of adsorbent performance in solid adsorption processes [4,5]. A systematic understanding of the CO_2 desorption step and regeneration behavior under different operating conditions is essential for selecting suitable adsorbents and optimising regeneration strategies for various CO_2 capture applications, thereby improving the economic and energy efficiency of adsorption-based separation processes.

Solid CO_2 adsorbents in common use includes X-type zeolite such as JLPM-3, 13X and its modifications, A-type zeolite such as 5A and 4A and carbon molecular sieves such as CMS-220, CMS-240 and CMS-260 [6-9]. Kareem *et al.* [10] reported that 13X zeolite adsorbed 5.226 mmol g^{-1} of CO_2 at 50 ºC. They further concluded that the heat of adsorption reflects the strength of the interaction between CO_2 molecules and the adsorbent framework. A lower heat of adsorption facilitates faster and more energy-efficient adsorbent regeneration. Sun *et al.* [11] reported that JLOX-500 exhibited higher CO_2 adsorption capacity and selectivity than 13X, which was attributed to its lower Si/Al ratio, larger specific surface area and pore volume and smaller pore size. Mendes *et al.* [12] and Hwang *et al.* [13] investigated the adsorption performance of

4A and 5A zeolites for CO_2 and CH_4 separation from flue gas, respectively. Both studies demonstrated that these zeolites exhibit a significantly higher affinity for CO_2 than CH_4, with adsorption capacity closely related to the adsorbent's polarisation characteristics. Song *et al*. [14] examined the influence of pore structure and surface chemistry on the CO_2 adsorption capacity and selectivity of three carbon molecular sieves. The results indicated that CO_2 and CH_4 adsorption capacities are primarily governed by the specific surface area and micropore volume. Similarly, Siriwardane *et al*. [15] reported that a larger volume of narrow micropores enhances CO_2 adsorption, with micropores smaller than 0.48 nm playing a dominant role in determining adsorption capacity. Sarker *et al*. [9] investigated the equilibrium and kinetic characteristics of CO_2 adsorption on 13X, 5A and MSC-3R carbon molecular sieves. They found that 13X and 5A zeolites possess a stronger affinity for CO_2 than carbon molecular sieves, whereas carbon molecular sieves exhibit higher CO_2 mass-transfer coefficients at low pressures.

In addition to adsorption performance, considerable attention has also been devoted to adsorbent regeneration using thermal, vacuum and purge-gas techniques. However, most studies have focused either on the regeneration time required to achieve complete desorption or on the regeneration efficiency under specific operating conditions. Comprehensive investigations of the CO_2 desorption process and the factors governing regeneration performance under different regeneration modes remain limited. Yassin *et al*. [16] compared the regeneration performance of 13X zeolite and activated carbon using microwave heating and conventional thermal regeneration with N_2 purging following CO_2/N_2 separation. Microwave heating significantly enhanced the CO_2 desorption rate of 13X, while activated carbon exhibited more stable regeneration efficiency under microwave irradiation. The regeneration stability of 13X was found to be comparable under both heating methods. Clausse *et al*. [17] investigated the combined effects of regeneration temperature and N_2 purge flow rate during CO_2 desorption and reported that the specific energy consumption initially decreased and subsequently increased with increasing temperature due to the existence of an optimum regeneration temperature. Vogtenhuber *et al*. [18] further demonstrated that purge-gas velocity had little influence on the cyclic regeneration performance at a regeneration temperature of 100 ºC. Jiang *et al*. [19] reported that combining vacuum with thermal regeneration reduced energy consumption compared with thermal regeneration alone. Santos *et al*. [20] observed that extending the purge duration improved product purity, whereas Punpee & Phalakornkule [21] found that 13X exhibited both higher CO_2 adsorption capacity and faster desorption kinetics than 5A under N_2 purging.

The economic viability of adsorption-based gas separation processes depends largely on the efficiency of adsorbent regeneration. However, most of the previous studies have evaluated the regeneration performance of individual adsorbents or compared specific regeneration techniques, while systematic investigations of the desorption behaviour of structurally distinct adsorbents under different regeneration driving forces (heating, purge gas and vacuum) remain scarce. This know-ledge gap limits the rational selection of adsorbents and regeneration strategies. Therefore, this study establishes a unified framework to systematically investigate the regeneration behaviour of three representative adsorbent classes *viz*. X-type zeolite (13X), A-type zeolites (4A and 5A) and carbon molecular sieve (CMS-240). The effects of thermal, purge-gas and vacuum regeneration are evaluated independently to investigate the influence of intrinsic adsorbent properties and external operating parameters on CO_2 desorption performance. The findings provide practical guidance for adsorbent selection and regeneration process design in diverse CO_2 capture and decarbonisation applications.

EXPERIMENTAL

Gas cylinders and molecular sieves: Carbon dioxide (CO_2) and methane (CH_4) with a purity of 99.999% were supplied by Qingdao Xinkeyuan Gas Co., Ltd. The gases were introduced into the experimental system through pressure-reducing valves. Commercial 13X, 4A and 5A zeolites, along with carbon molecular sieve (CMS-240), were procured from Luoyang Jianlong Micro Nano New Materials Co., Ltd. and Jiangxi Xintao Technology Co., Ltd. The physico-chemical properties of the adsorbents are summarised in Table-1. The properties of 13X were experimentally characterised in this study, whereas those of 4A, 5A and CMS-240 were obtained from the literature.

Estimation of CO_2 adsorption and desorption characteristics

Experiment set-up and operation methods

Experiment system set-up: The experimental setup for CO_2 adsorption and desorption on solid adsorbents is shown in Fig. 1. The system was constructed based on the static volume adsorption method. CO_2 desorbed *via* heating was conducted by heating the adsorption column with an electrically heated steel jacket, CO_2 desorbed *via* vacuuming was achieved by connecting a vacuum pump at the column outlet and CO_2 desorbed *via* purging was operated by connecting a gas cylinder and a flow meter at the inlet of the adsorption column. The length of adsorption and reference columns was 200 mm, the inner diameter was 25 mm. The temperature control device

TABLE-1
CHARACTERISTICS OF ZEOLITE-4A, 5A, 13X AND CMS-240 [22,23]

Adsorbent	Framework	Cation location	Cation type	Average pore size (nm)
CMS-240	No crystal structure and cation and the internal pore are connected.		None	≈ 0.4
13X	Truncated octahedron structure, hexagonal prisms connect each unit.	Every unite cell has positons of 16 I, 3I', 32II, 32II', 48III, 48III'	Na^+	≈ 2.1
4A	Truncated octahedron structure, quaternary prisms connect each unit.	Every unite has positions of 8I, 3II, 12III.	Na^+	≈ 0.42
5A			Ca^{2+}	≈ 0.49

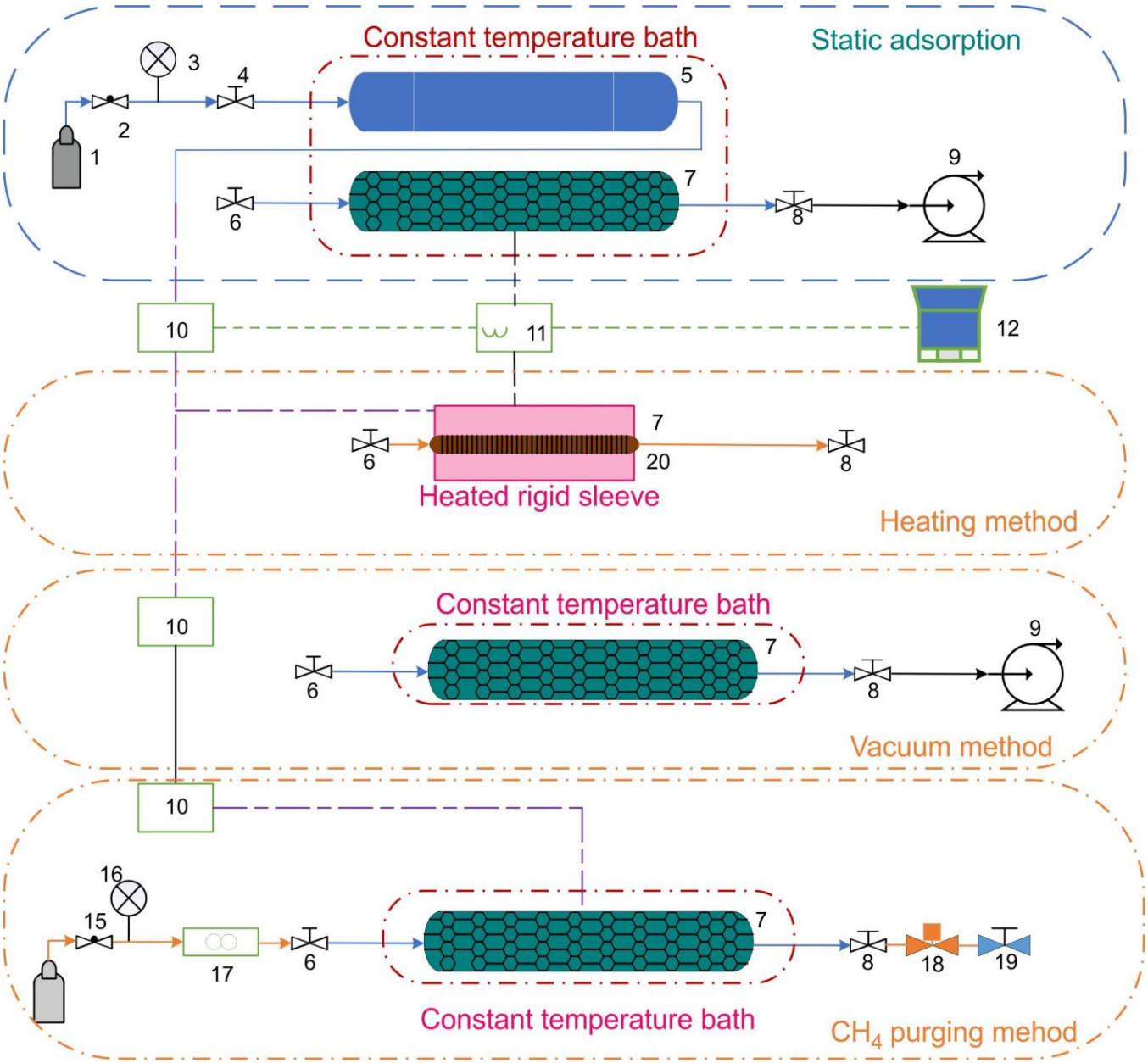

Fig. 1. Experimental system (1,14 CO_2 and CH_4 cylinders; 2,15 pressure reducing valve; 3,16 pressure gauges; 4,6,8 needle valve; 5 reference column; 7 adsorption column; 9 vacuum pump; 10 pressure sensor; 11 temperature sensor; 12 data-collection service; 17 gas mass flow controller; 18 back pressure valve; 19 blowoff valve)

includes a thermostatic water bath and an electrically heated steel jacket. The thermostatic water bath (HH-60 Qingdao Chuanghesheng Scientific and Educational Instrumentation Co., Ltd.) controls temperature up to 100 ºC. The electrically heated steel jacket can control temperature up to 500 ºC, with a control accuracy of ± 0.5 ºC. Detection system includes a pressure sensor with 0~6 MPa and accuracy of 0.25% F.S., a temperature sensor with 0~1100 ºC and a mass flow controller with flow control range of 0~3 MPa. The experimental system was equipped with a pressure sensor (0-6 MPa, accuracy ± 0.25% full scale), a temperature sensor (0-1100 ºC) and a mass flow controller with a flow rate range of 0-3 L min^{-1}. The mass flow controller operated over a differential pressure range of 0.2-0.8 MPa and a backpressure range of 0-800 psi.

Thermodynamic properties measurement: The CO_2 adsorption isotherms were determined using the static volumetric method prior to regeneration. The specifications of the adsorbents used in the experiment are shown in Table-2. Before the experiment, the adsorbent samples were placed in a vacuum tube furnace and activated at 380 ºC for 2 h to remove moisture and adsorbed impurities; they were then cooled to room temperature under vacuum. High-purity CO_2 (99.999%) was used as the adsorbate and adsorption was carried out at different equilibrium pressures. Before adsorption, evacuate the entire system before back-flushing the column. Wait until the temperature and pressure have remained constant for at least 30 min before conducting the experiment. For each pressure point, record the pressure before and after adsorption after

ensuring that the system pressure has fluctuated by less than 0.1 kPa for at least 10 min. The CO_2 adsorption capacity and heat of adsorption were calculated using eqns. 1 and 2, respectively. Once adsorption is complete, close the inlet and outlet valves of the adsorption column and switch to the specified regeneration mode.

TABLE-2
SPECIFICATION OF STUDIED ZEOLITES FOR THIS EXPERIMENT

Molecular sieve	Shape	Particle size (mm)
13X	Spherical	3~5
CMS-240	Striped	1.3
5A	Spherical	1.7~2.5
4A	Spherical	1.7~2.5

CO_2 desorption experiment: During CO_2 desorption experiments, solid adsorbents regenerated *via* heating was realised by the electrically heated rigid sleeve attached to the outer wall of the adsorption column. Vacuum method was operated by a pump connecting to adsorption column. Adsorbents regenerated *via* purging was operated through a purge gas cylinder connected to the inlet of the adsorption column. The mass of empty column, the mass of column after loading molecular sieve and the mass of column after vacuuming were measured by a high-precision electronic balance before doing CO_2 desorption experiment. Then, the column was put into a thermostatic water bath to keep warm.

In vacuuming experiment, the vacuum pressure of pump was set and then the saturated molecular sieve was regenerated by vacuum pumping, vacuum pump was turned off when the set time was reached. For the purge-gas regeneration experiments, the purge gas flow rate was set at the desired value and the cylinder pressure was regulated to 0.2 MPa. The adsorption column was removed after the prescribed purging time, weighed, and then returned to the system for continued purging. This procedure was repeated until a total regeneration time of 60 min was reached. For the thermal regeneration experiments, the adsorption column was placed inside an electrically heated sleeve and heated to the desired temperature to facilitate CO_2 desorption. The adsorption column was removed and weighed at predetermined time intervals to monitor the desorption process. The CO_2 desorption rate and desorption ratio were calculated using eqns. 3 and 4, respectively.

Calculation of indexes

CO_2 adsorption amount:

$$n_n = n_{n-1} + \frac{1}{R}\left[\frac{P_n V_r}{Z_n T_r} + P'_{n-1}\frac{V_n}{Z'_{n-1}T_n} - P'_n\left(\frac{V_r}{Z'_n T_r} + \frac{V_n}{Z'_n T_n}\right)\right] \quad (1)$$

where n_{n-1} is CO_2 adsorbed amount at n_{n-1} pressurisation (mol); T_r and T_n are temperature of the reference and equilibrium adsorption columns, respectively (K); V_r and V_n are the volume of the reference column and the free volume of the equilibrium adsorption column after putting in the adsorbent, respectively (m^3); P_n and P'_n the reference column pressure and system equilibrium pressure after the n pressurisation (Pa), Z_n and Z'_n are the compression factors at the reference column pressure and at the equilibrium pressure of the system after the n pressurisation, P'_{n-1} and Z'_{n-1} are the compression factors at the n – 1 system equilibrium pressure and system equilibrium pressure and R is the universal gas constant.

Heat of adsorption calculation: The heat of CO_2 adsorption on the solid adsorbents was determined using the Van't Hoff equation, which describes the relationship between temperature and the Henry's law constant (K_H) (eqn. 2). By transforming the Van't Hoff equation into its logarithmic form, the heat of adsorption (ΔH) was obtained from the linear relationship between ln K_H and the reciprocal of the absolute temperature (T^{-1}).

$$K_H = K_{H0} e^{\left(-\frac{\Delta H}{RT}\right)} \quad (2)$$

where K_H is Henry's law constant (mmol g^{-1} kPa^{-1}); K_{H0} is parameter of the Van't Hoff equation (mmol g^{-1} kPa^{-1}); ΔH is heat of adsorption (J mol^{-1}); T is temperature (K). In this study, the Henry's constant values for CO_2 on 13X, 4A, 5A and CMS-240 are shown in Table-3.

TABLE-3
HENRY'S CONSTANT VALUES FOR CO_2 ON 13X, 4A, 5A AND CMS-240 MOLECULAR SIEVES

Adsorbents	K_H (mmol g^{-1} kPa^{-1})		
	30 ºC	50 ºC	70 ºC
13X	0.2087	0.1225	0.0747
5A	0.3248	0.1928	0.1175
4A	0.2052	0.1067	0.0554
CMS-240	0.0213	0.0140	0.0102

Calculation of CO_2 desorption volume and desorption rate: In this study, the gravimetric method was employed to determine the amount of CO_2 desorbed from the solid adsorbents. The regeneration performance under different operating conditions was evaluated using the CO_2 desorption amount and CO_2 desorption rate, as defined by eqns. 3 and 4, respectively.

$$q_{des} = q_1 - \frac{(m_3 - m_1)\times 10^3}{(m_2 - m_0)\times 44} \quad (3)$$

where q_{des} = CO_2 desorption from molecular sieves (mmol g^{-1}); q_1 = saturated adsorption capacity of the molecular sieve at this pressure (mmol g^{-1}); m_0 = mass of molecular sieves contained in vacuum (g); m_1 = mass of empty column before adsorption (g); m_2 = total mass of the system before adsorption (g); m_3 = total mass of the system after regeneration (g).

$$\eta\ (\%) = \frac{q_1 - q_2}{q_1}\times 100 \quad (4)$$

where η = CO_2 desorption rate of the molecular sieve, q_2 = total adsorbed amount after desorption (mmol g^{-1}).

RESULTS AND DISCUSSION

Adsorption thermodynamics characteristics: As shown in Fig. 2, the CO_2 adsorption isotherms and heat of adsorption of 13X, 5A, 4A and CMS-240 were determined. Among the four isotherm models evaluated (Langmuir, Freundlich, Toth and Sips), the Sips model provided the best fit to the

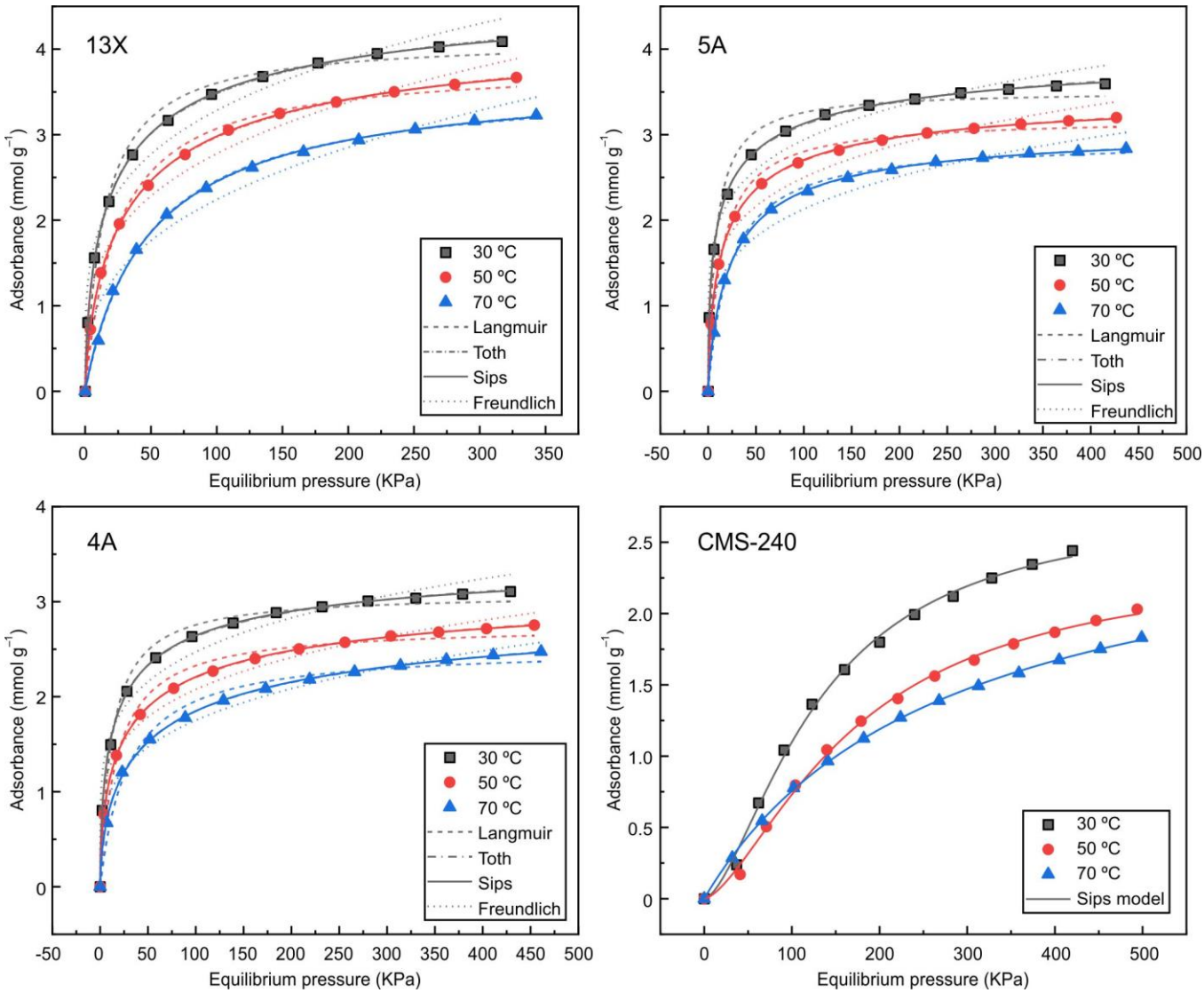

Fig. 2. CO_2 adsorption isotherms at 13X, 5A, 4A and CMS-240 molecular sieves, respectively

experimental data for all adsorbents (Tables 4 and 5). Therefore, the parameters obtained from the Sips model were used to calculate the heat of CO_2 adsorption.

By combining the adsorption data with the structural characteristics of the adsorbents (Table-1), it is evident that the heat of adsorption does not necessarily correlate with the

TABLE-4
ADSORPTION MODEL PARAMETERS OF CO_2 ON 13X, 5A AND 4A MOLECULAR SIEVES

Model	Temp. (°C)	q_m (mmol g^{-1})			k (kPa^{-1})			n			R^2		
		13X	5A	4A	13X	5A	4A	13X	5A	4A	13X	5A	4A
Langmuir	30	4.12	3.52	3.09	0.06912	0.12756	0.08345	–	–	–	0.98721	0.97382	0.98231
	50	3.83	3.19	2.75	0.04059	0.07184	0.05540	–	–	–	0.99346	0.99015	0.96306
	70	3.64	2.93	2.52	0.02108	0.04321	0.03466	–	–	–	0.99921	0.99727	0.98568
Toth	30	5.24	4.52	3.81	0.21225	1.17913	0.42425	0.49222	0.38986	0.45342	0.99987	0.99946	0.99925
	50	4.68	3.71	3.61	0.07840	0.18848	0.26882	0.58075	0.55812	0.43489	0.99990	0.99998	0.99997
	70	3.77	3.18	3.52	0.02243	0.06335	0.13509	0.91044	0.73446	0.43384	0.99938	0.99990	0.99973
Sips	30	4.86	4.18	3.58	0.04295	0.07710	0.05731	1.54589	1.87331	1.68328	0.99988	0.99987	0.99963
	50	4.40	3.56	3.33	0.02784	0.05416	0.03204	1.37593	1.47086	1.71297	0.99988	0.99990	0.99995
	70	3.71	3.12	3.17	0.02014	0.03765	0.01749	1.04122	1.21805	1.67130	0.99931	0.99981	0.99951
Freundlich	30	–	–	–	1.06368	1.27142	1.00378	4.08513	5.49298	5.11184	0.97307	0.97458	0.97394
	50	–	–	–	0.75400	0.95499	0.76578	3.53120	4.78615	4.61623	0.97697	0.96966	0.98208
	70	–	–	–	0.45205	0.70830	0.55009	2.87669	4.18652	3.97622	0.97102	0.96460	0.98

TABLE-5
SIPS ADSORPTION MODEL
PARAMETER OF CO_2 ON CMS-240

Model	Temp. (ºC)	q_m (mmol g^{-1})	k (kPa^{-1})	R^2
Sips	30	2.77	0.00770	0.99776
	50	2.39	0.00586	0.99817
	70	2.82	0.00362	0.99981

CO_2 adsorption capacity. Instead, it is strongly influenced by the framework structure and chemical composition of the adsorbent. Under the experimental conditions (30 ºC and 350 kPa), the saturated CO_2 adsorption capacities followed the order: 13X (4.089 mmol g^{-1}) > 5A (3.596 mmol g^{-1}) > 4A (3.108 mmol g^{-1}) > CMS-240 (2.442 mmol g^{-1}). In contrast, the heats of adsorption were followed the order as: 4A (28.26 kJ mol^{-1}) > 13X (22.20 kJ mol^{-1}) > 5A (21.98 kJ mol^{-1}) > CMS-240 (15.92 kJ mol^{-1}).

CMS-240, which lacks a crystalline framework and exchangeable cations, exhibited both the lowest CO_2 adsorption capacity and the lowest heat of adsorption. In contrast, the crystalline zeolites (13X, 4A and 5A) demonstrated higher adsorption capacities owing to their well-defined pore structures and cationic adsorption sites (Table-5). Although 13X exhibited the highest CO_2 adsorption capacity, its heat of adsorption was considerably lower than that of 4A. A similar trend was observed for 5A confirmed that CO_2 adsorption capacity and the heat of adsorption are controlled by different factors. CO_2 adsorption capacity is mainly influenced by the pore structure and the availability of adsorption sites, whereas the heat of adsorption depends largely on the interaction strength between CO_2 molecules and the adsorbent framework. These results are consistent with those reported by Khoramzadeh *et al*. [24].

CO_2 desorption performance *via* heating: In practical applications, the regeneration temperature is generally limited to below 300 ºC to avoid damage to the pore structure of the adsorbent. Therefore, regeneration temperatures of 150, 200 and 250 ºC were selected to investigate the thermal desorption performance of CO_2.

The CO_2 desorption profiles of the four adsorbents are presented in Fig. 3. Effective regeneration was achieved at all three temperatures (150-250 ºC). More than 80% of the

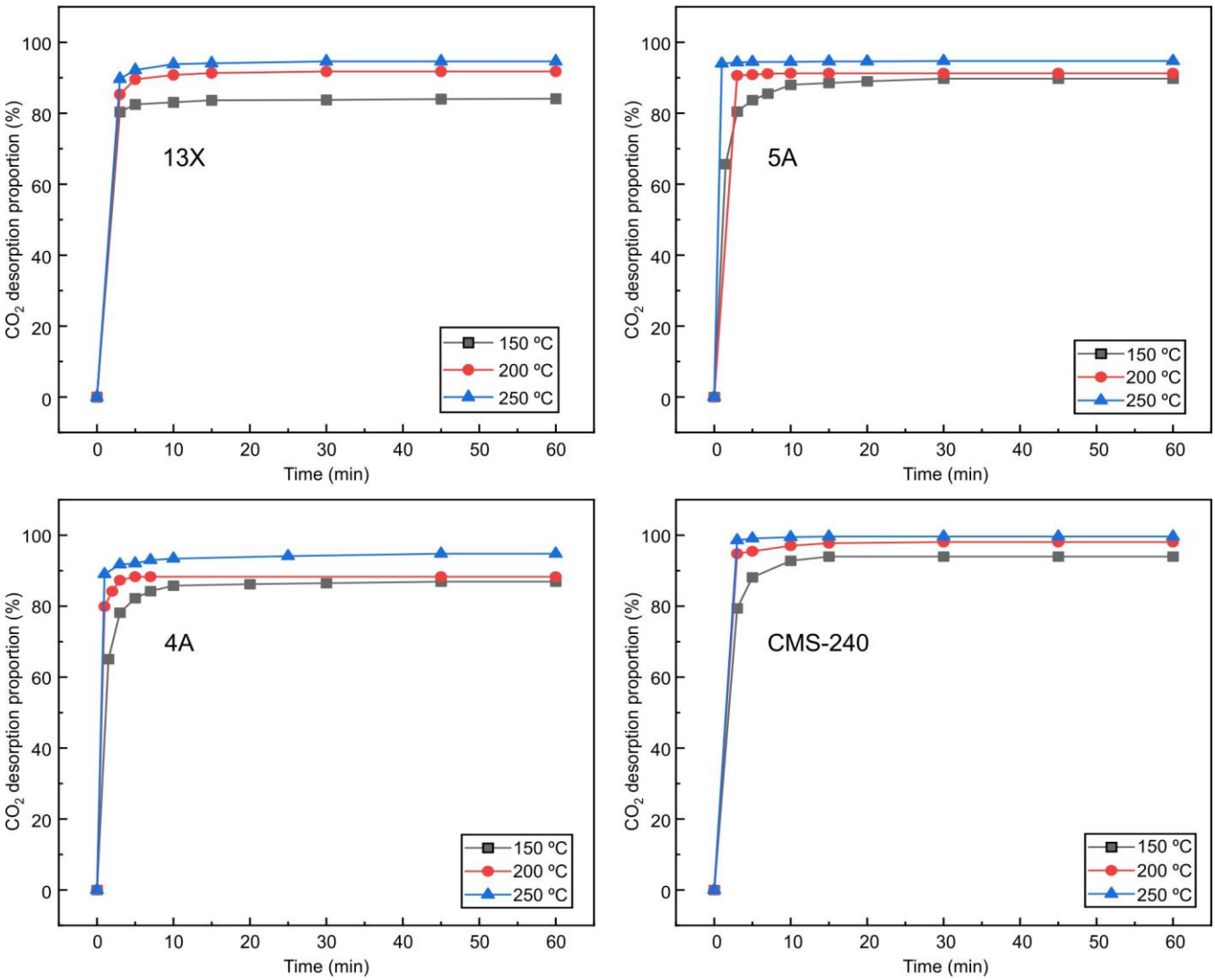

Fig. 3. Effect of regeneration temperature (150, 200 and 250 ºC) on the CO_2 desorption behaviour of molecular sieves 13X, 5A, 4A and CMS-240

adsorbed CO_2 was desorbed within the first 5-10 min, while desorption efficiencies exceeding 90% were obtained after 5-10 min of heating at 200 and 250 ºC. The results also revealed a close relationship between the heat of adsorption and regeneration performance. CMS-240 exhibited the lowest heat of adsorption (15.92 kJ mol^{-1}) and consequently the fastest CO_2 desorption rate and the highest desorption efficiency, with the desorption ratio exceeding 90% under all heating conditions. In contrast, 13X and 5A showed similar heats of adsorption (22.20 and 21.98 kJ mol^{-1}, respectively) and correspondingly lower desorption rates than CMS-240. Among the 4 adsorbents, 4A possessed the highest heat of adsorption and exhibited the slowest CO_2 desorption, with a maximum desorption ratio of only approximately 90%.

CO_2 desorption performance *via* vacuuming: CO_2 desorption under vacuum was investigated at absolute pressures of 100, 80 and 60 kPa for 10 min at 30 ºC. As shown in Fig. 4, vacuum pressure had a pronounced influence on the regeneration performance of the adsorbents. A pressure of 60 kPa produced the highest desorption efficiency, followed by 80 kPa and 100 kPa, reflecting the stronger driving force for desorption at lower pressures. Under vacuum regeneration, the maximum CO_2 desorption ratios of CMS-240, 13X, 4A, and 5A were approximately 90%, 80%, 50% and 45%, respectively, all of which were lower than those achieved by thermal regeneration.

CMS-240 reached a CO_2 desorption ratio of approximately 90% within the first 5 min, after which the desorption profile approached a plateau with little further change. For 13X, the desorption ratio increased from approximately 70% at 5 min to 80% after 10 min. In contrast, the desorption ratios of 4A and 5A remained below 50% throughout the regeneration period, with 4A consistently exhibiting values approximately 5% higher than those of 5A.

The superior vacuum regeneration performance of CMS-240 can be attributed to both its pore structure and surface chemistry. Unlike zeolites, CMS-240 does not possess a crystalline aluminosilicate framework with well-defined pore windows. Its interconnected pore network provides relatively low diffusion resistance, allowing CO_2 molecules to diffuse rapidly from the adsorbent during the initial stage of desorption [25]. Nevertheless, the bottle-neck pore structure within its narrow micropores can hinder the release of a small fraction of strongly confined CO_2 molecules, resulting in a

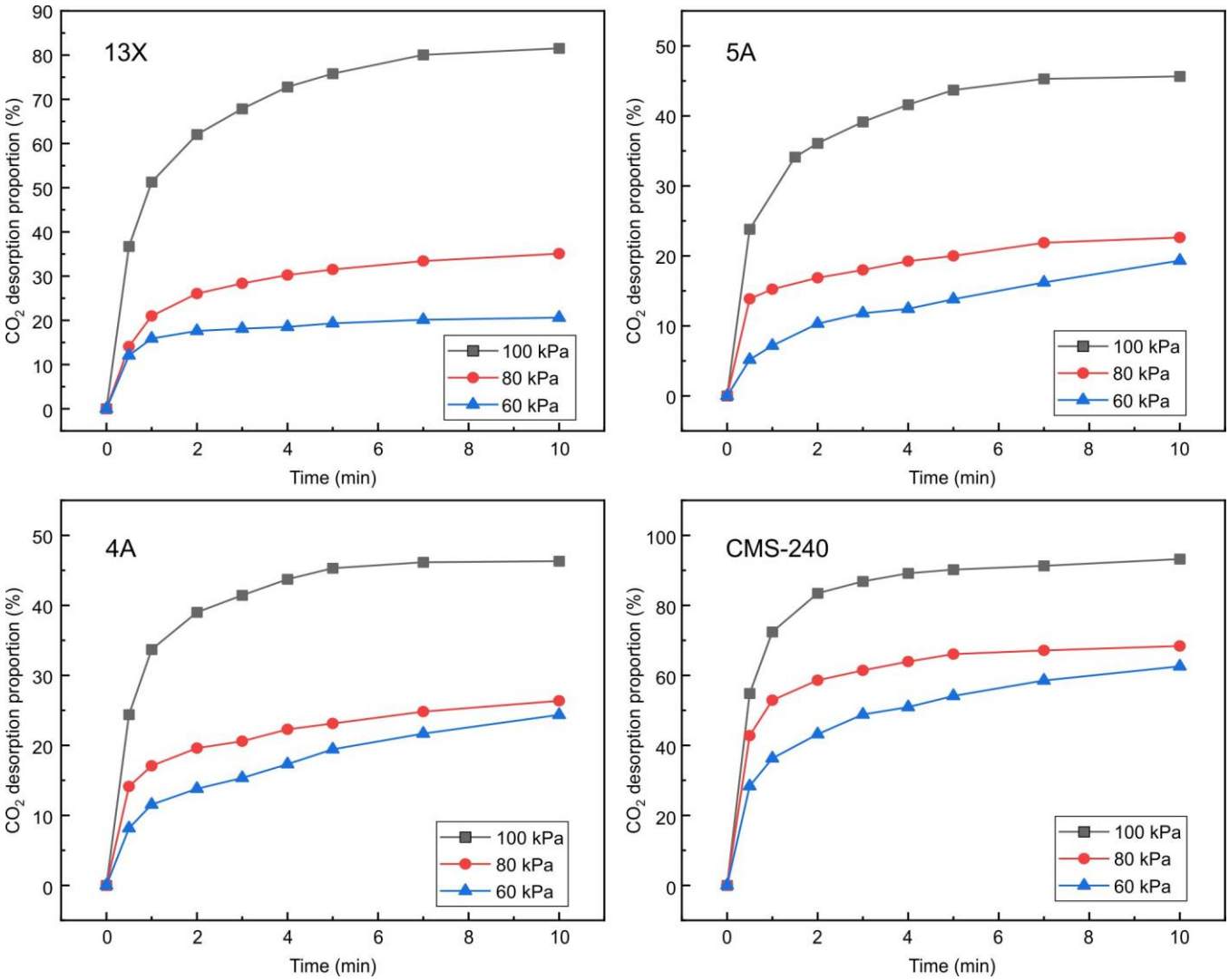

Fig. 4. Time-dependent CO_2 adsorption profiles of molecular sieves 13X, 5A, 4A and CMS-240 at adsorption pressures of 60 80 and 100 kPa

slower final stage of desorption. From a chemical perspective, carbon molecular sieves lack the exchangeable cations present in zeolites, thereby eliminating the strong electrostatic interactions between CO_2 molecules and cationic adsorption sites that hinder desorption. This interpretation agrees with previous study [25]. In addition, a high concentration of oxygen-containing surface functional groups may strengthen the interaction with CO_2, thereby prolonging the desorption process.

Among the zeolites, 13X exhibited substantially better regeneration performance than 4A and 5A. Its larger average pore diameter (approximately 2.1 nm) facilitates the diffusion of CO_2 from both the adsorption sites and the pore network, leading to a higher desorption ratio. This observation is consistent with the results reported by Montanari & Busca [26].

Combining the regeneration results with the structural characteristics of the adsorbents demonstrates that the crystal structure strongly influences CO_2 desorption under vacuum conditions. Adsorbents with open pore networks and lower diffusion resistance exhibit faster and more efficient desorption. For adsorbents with similar framework structures, the type and concentration of exchangeable cations further affect regeneration performance. Lower cation density and lower cation charge reduce the electrostatic attraction between CO_2 molecules and the adsorption sites, thereby promoting CO_2 desorption.

CO_2 desorption performance *via* CH_4 purging: In industrial pressure swing adsorption (PSA) processes, the purge-to-feed ratio (P/F) typically ranges from 0.08 to 0.16, with feed gas flow rates of 1000-1500 mL min^{-1} under elevated operating pressures [27]. Purge gas flow rates of 50, 100, and 200 mL min^{-1} were selected to investigate their effect on CO_2 desorption.

Fig. 5 presents the CO_2 desorption behaviour of the four adsorbents during purge-gas regeneration. CMS-240, which lacks a crystalline framework, exhibited the highest regeneration efficiency. At purge flow rates of 100 and 200 mL min^{-1}, the CO_2 desorption ratio exceeded 90%. The maximum desorption ratios of 13X, 4A and 5A remained below approximately 70%, 60% and 60%, respectively. The same behaviour was observed during vacuum regeneration.

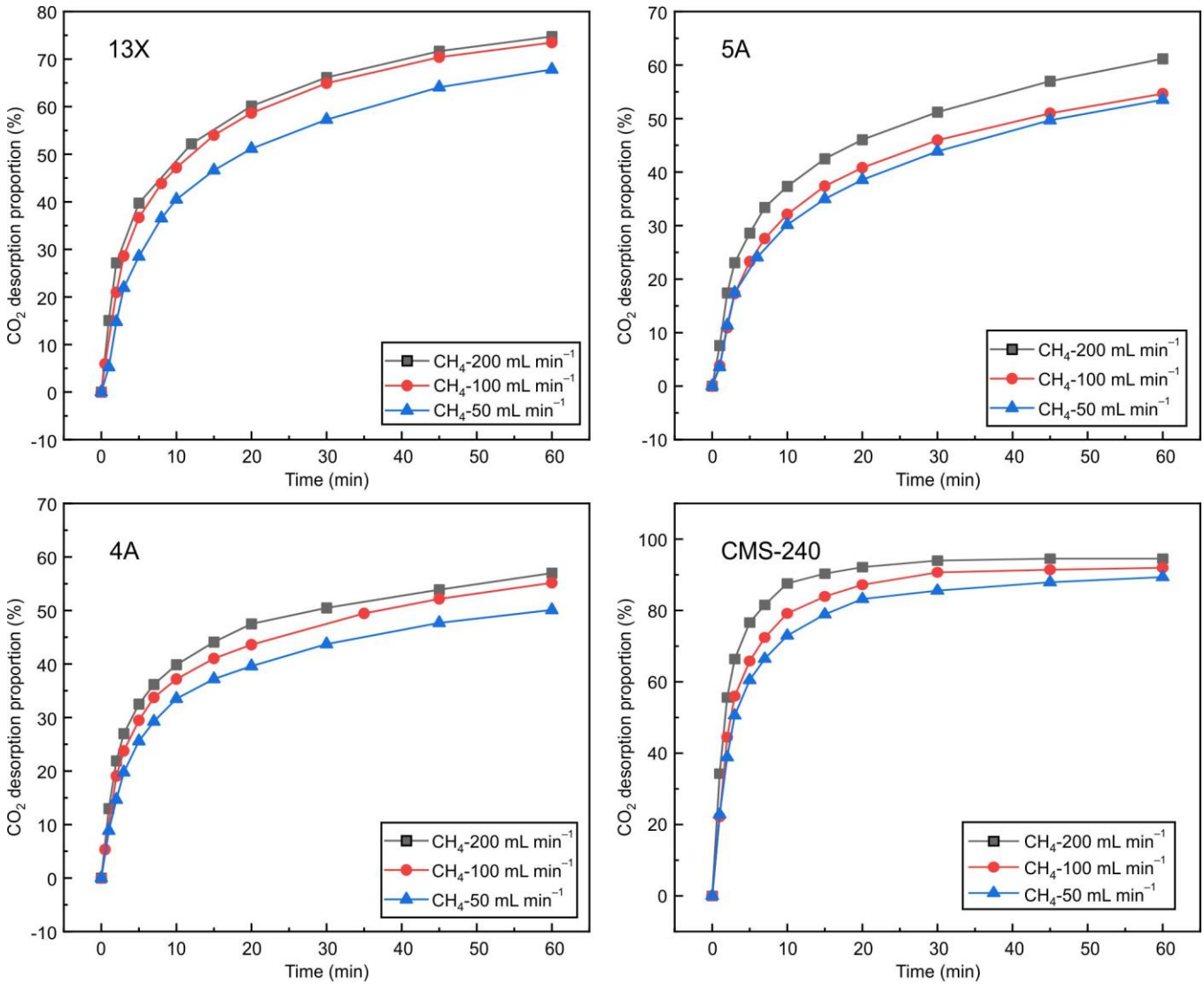

Fig. 5. Variation of CO_2 adsorption capacity with adsorption time for molecular sieves 13X, 5A, 4A and CMS-240 at different gas flow rates (50, 100 and 200 mL min^{-1})

The purge gas flow rate had little influence on CO_2 desorption during the first 10 min of regeneration. A higher flow rate accelerated desorption after 10 min. Purge gas lowers the CO_2 partial pressure inside the adsorption column, developing the driving force required for CO_2 desorption. The continuous gas flow removes desorbed CO_2 from the adsorbent surface and reduces mass-transfer resistance [21]. At the beginning of regeneration, CO_2 molecules weakly adsorbed on the surface or located in large and mesopores desorb readily. As regeneration continues, the remaining CO_2 is retained within narrow micropores or at cationic adsorption sites, where stronger interactions require a larger driving force for desorption. Higher purge gas flow rates are therefore more effective during the middle and final stages of regeneration.

The final regeneration efficiency depended primarily on the total volume of purge gas rather than the purge flow rate or regeneration time considered independently. The CO_2 desorption ratio of 13X after 30 min at 100 mL min^{-1} was nearly identical to that obtained after 60 min at 50 mL min^{-1}. Tlili *et al*. [28] reached the same conclusion, reporting that the regeneration degree of solid adsorbents is governed mainly by the total purge gas volume.

Fig. 6 compares the regeneration performance of the four adsorbents under thermal, vacuum and purge-gas regeneration. CMS-240 achieved CO_2 desorption ratios exceeding 90% under all three regeneration methods. Thermal regeneration provided the highest desorption efficiency for the crystalline zeolites. For 13X, the desorption ratios obtained by thermal and vacuum regeneration differed by less than 5%. For 4A and 5A, thermal regeneration achieved desorption ratios approaching 95%, whereas vacuum and purge-gas regeneration remained below 60%.

The desorption curves of 4A and 5A obtained by vacuum and purge-gas regeneration intersected at approximately 20 min. Vacuum regeneration yielded a higher desorption rate during the initial stage due to the larger pressure gradient. Purge-gas regeneration became more effective after approximately 20 min. This crossover was not observed for 13X. The difference is closely related to the pore structure of the zeolites. The pore openings of 4A and 5A (~ 0.5 nm) are much

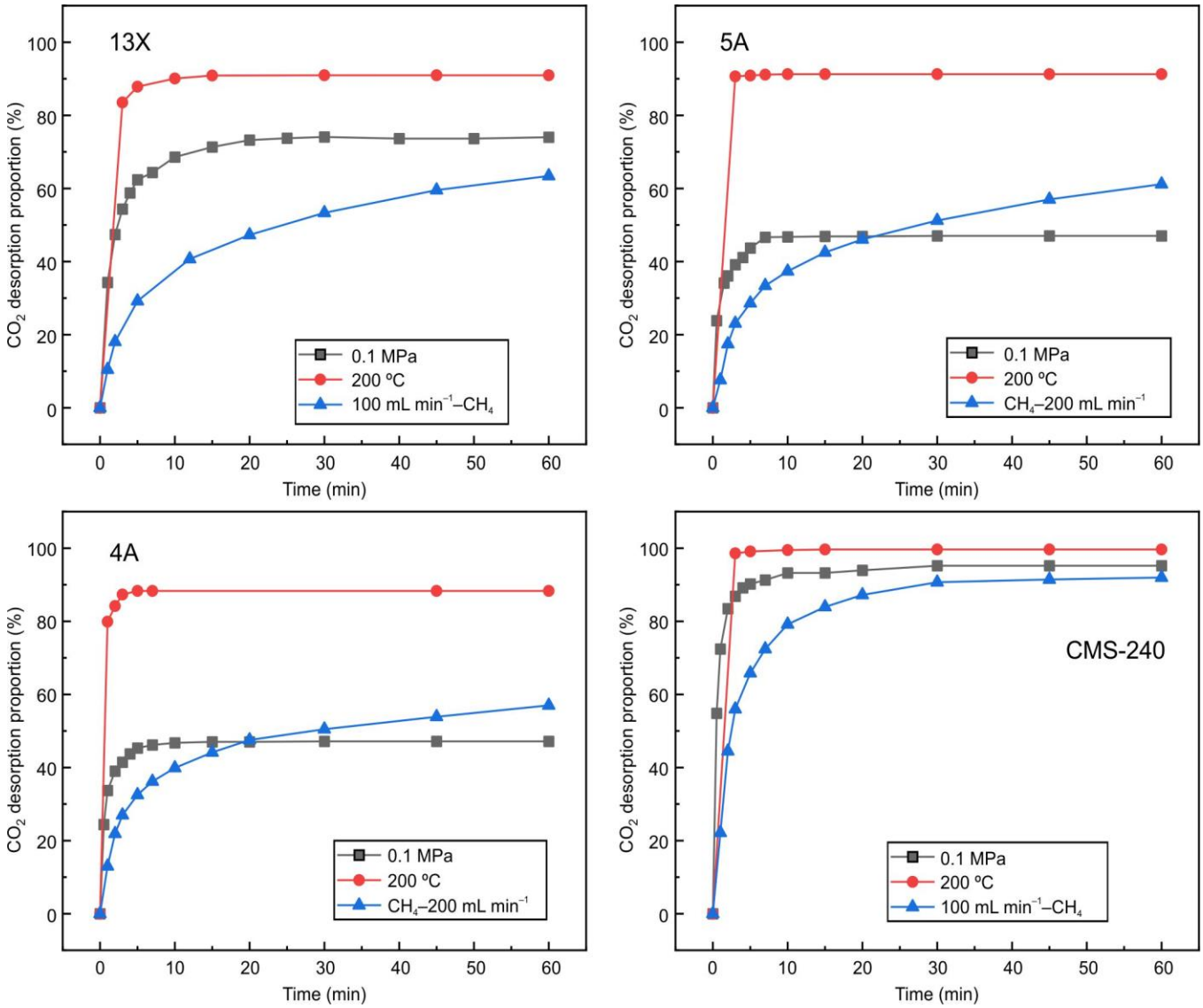

Fig. 6. Comparison of regeneration characteristics of adsorbent under different regeneration methods

smaller than those of 13X (~ 2.1 nm). During the initial stage, the strong pressure gradient generated by vacuum removes CO_2 rapidly from readily accessible adsorption sites. As desorption progresses, the remaining CO_2 becomes confined within narrow micropores and interacts strongly with exchangeable cations. The continuous sweeping action of the purge gas supplies additional mass-transfer driving force, facilitating the removal of the residual CO_2, in agreement with the observations reported by Jiang *et al*. [29].

Thermal regeneration achieved high CO_2 desorption efficiencies for all four adsorbents. Vacuum and purge-gas regeneration were less effective for the crystalline A-type and X-type zeolites. The regeneration behaviour of these zeolites was influenced more strongly by pore size than by differences in cation type or cation density under the conditions investigated.

Effect of regeneration mode on CO_2 desorption characteristics: CO_2 desorption efficiency alone is insufficient for evaluating adsorbent performance. The CO_2 working capacity is equally important since it determines the amount of CO_2, which can be captured and released during each adsorption–desorption cycle. Fig. 7 presents the repeatability errors together with the maximum adsorption capacities, desorption capacities and working capacities under the optimum regeneration conditions. Under thermal regeneration at 200 ºC, the working capacities followed the order: 13X (3.650 mmol g^{-1}) > 5A (3.363 mmol g^{-1}) > 4A (2.803 mmol g^{-1}) > CMS-240 (2.569 mmol g^{-1}). Under vacuum regeneration at 100 kPa, the working capacities were 13X (3.291 mmol g^{-1}) > CMS-240 (2.383 mmol g^{-1}) > 5A (1.679 mmol g^{-1}) > 4A (1.482 mmol g^{-1}). During CH_4 purge-gas regeneration at 100 mL min^{-1}, the working capacities followed the order: 13X (2.938 mmol g^{-1}) > CMS-240 (2.286 mmol g^{-1}) > 5A (2.026 mmol g^{-1}) > 4A (1.760 mmol g^{-1}).

CMS-240 exhibited the highest CO_2 desorption efficiency but a lower working capacity as it lacks the abundant adsorption sites provided by exchangeable cations in zeolites. The 13X framework contains numerous cationic adsorption sites (16I, 32I′, 32II, 32II′, 48III and 48III′ per unit cell), which strengthen the electrostatic interaction with the highly polar

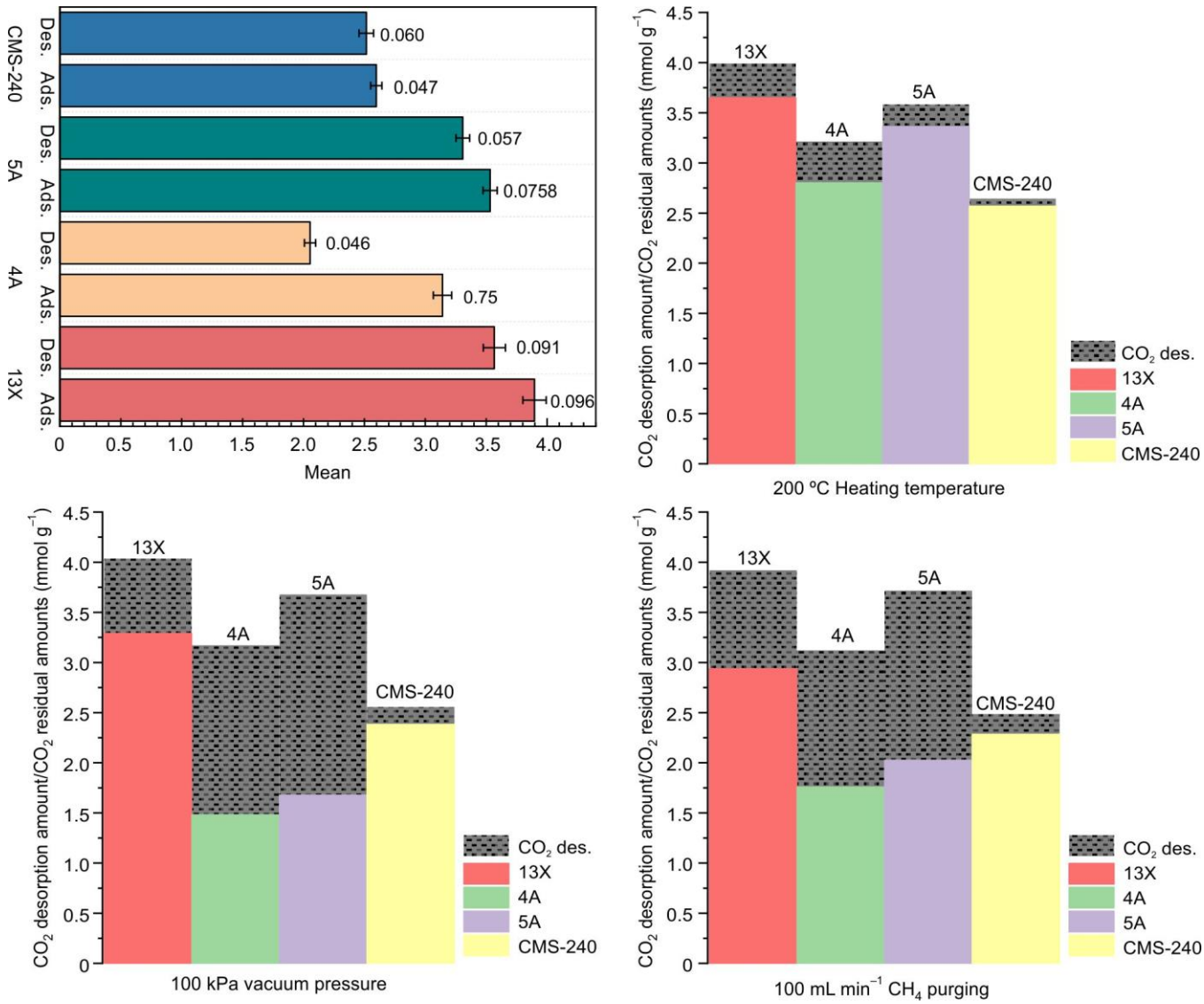

Fig. 7. Comparison of working capacity of molecular sieve under different regeneration methods

CO_2 molecules and result in a much higher adsorption capacity. The stronger adsorption interactions increase the energy required for desorption, creating a trade-off between adsorption capacity and regeneration efficiency. Practical process design should balance these two factors according to the requirements of the target CO_2 capture application including feed gas composition, regeneration energy demand and product purity. CMS-240 is well suited to applications where regeneration energy is the primary consideration or where CO_2 partial pressures are low, such as direct air capture. The higher working capacity of 13X makes it more attractive for treating gas streams with relatively high CO_2 concentrations. The larger average pore diameter of 13X (2.1 nm), compared with those of 4A and 5A (0.42-0.49 nm), also contributes to its superior regeneration performance among the zeolite adsorbents.

Conclusion

This study systematically investigated the CO_2 desorption behaviour of 13X, 4A, 5A and CMS-240 under thermal, vacuum and CH_4 purge-gas regeneration. CMS-240 achieved CO_2 desorption ratios above 90% under all regeneration conditions, whereas 4A exhibited the lowest regeneration efficiency due to its high heat of adsorption (28.26 kJ mol^{-1}). Among the zeolites, pore size exerted a greater influence on regeneration performance than cation type. During CH_4 purge-gas regeneration, the final CO_2 desorption ratio depended primarily on the total purge-gas volume rather than the purge flow rate or regeneration time. Under thermal regeneration at 200 ºC, 13X exhibited the highest working capacity (3.650 mmol g^{-1}), followed by 5A (3.363 mmol g^{-1}), 4A (2.803 mmol g^{-1}) and CMS-240 (2.569 mmol g^{-1}). Thermal regeneration was the most effective regeneration method for all adsorbents. The high CO_2 working capacity and favorable regeneration performance of 13X make it a suitable adsorbent for industrial CO_2 capture and separation.

ACKNOWLEDGEMENTS

This work was supported by Innovation fund project for graduate student of China University of Petroleum (East China) (Grant No. 23CX04039A), the Fundamental Research Funds for the Central Universities (Grant No. 23CX04039A).

CONFLICT OF INTEREST

The authors declare that there is no conflict of interests regarding the publication of this article.

DECLARATION OF AI-ASSISTED TECHNOLOGIES

During the preparation of this manuscript, the authors used an AI-assisted tool(s) to improve the language and no data, results or scientific conclusions were generated by AI. All analyses, interpretations and conclusions are the authors' own. The authors reviewed and edited the content and take full responsibility for the published work.

REFERENCES

1. L. Gómez, I. Martínez, M. V. Navarro, and R. Murillo, *J. CO2 Utiliz.*, **77**, 102611 (2023); https://doi.org/10.1016/j.jcou.2023.102611
2. P. Wu, A. Debebe, and Y. H. Ma, *Zeolites*, **3**, 118 (1983); https://doi.org/10.1016/0144-2449(83)90199-9
3. P.J.E. Harlick and F.H. Tezel, *Can. J. Chem. Eng.*, **79**, 236 (2001); https://doi.org/10.1002/cjce.5450790206
4. C. Ellison, J. Hoffman and D. Shekhawat, *Int. J. Greenh. Gas Control*, **107**, 103311 (2021); https://doi.org/10.1016/j.ijggc.2021.103311
5. R. Morales-Ospino, R.G. Santiago, R.M. Siqueira, D.C.S. de Azevedo and M. Bastos-Neto, *Adsorption*, **26**, 813 (2020); https://doi.org/10.1007/s10450-019-00192-5
6. J.S. Lee, J.H. Kim, J.T. Kim, J.K. Suh, J.M. Lee and C.H. Lee, *J. Chem. Eng. Data*, **47**, 1237 (2002); https://doi.org/10.1021/je020050e
7. M. Mofarahi and F. Gholipour, *Micropor. Mesopor. Mater.*, **200**, 1 (2014); https://doi.org/10.1016/j.micromeso.2014.08.022
8. D. Panda, E.A. Kumar and S.K. Singh, *J. CO2 Utiliz.*, **40**, 101233 (2020); https://doi.org/10.1016/j.jcou.2020.101223
9. A.I. Sarker, A. Aroonwilas and A. Veawab, *Energy Procedia*, **114**, 2450 (2017); https://doi.org/10.1016/j.egypro.2017.03.1394
10. F.A. Abdul Kareem, A.M. Shariff, S. Ullah, N. Mellon and L.K. Keong, *Micropor.Mesopor. Mater.*, **267**, 221 (2018); https://doi.org/10.1016/j.micromeso.2018.04.007
11. Y.B. Sun, J.F. Tang, G.Y. Li, Y.H. Hua, H. Li and S.Y. Hu, *ACS Omega*, **7**, 18542 (2022); https://doi.org/10.1021/acsomega.2c01211
12. P.A.P. Mendes, A.M. Ribeiro, K. Gleichmann, A.F.P. Ferreira and A.E. Rodrigues, *J. CO2 Util.*, **20**, 224 (2017); https://doi.org/10.1016/j.jcou.2017.05.003
13. K.J. Hwang, M.J. Hwang, M.S. Balathanigaimani, K. Nwe, Y. Youn, W.S. Choi, H.A. Kim, J.W. Nah and W.G. Shim, *Adsorption*, **25**, 833 (2019); https://doi.org/10.1007/s10450-019-00086-6
14. X. Song, L.A. Wang, X. Ma and Y.M. Zeng, *Appl. Surf. Sci.*, **396**, 870 (2017); https://doi.org/10.1016/j.apsusc.2016.11.050
15. R.V. Siriwardane, M.S. Shen, E.P. Fisher and J.A. Poston, *Energy Fuels*, **15**, 279 (2001); https://doi.org/10.1021/ef000241s
16. M.M. Yassin, J.A. Anderson, G.A. Dimitrakis and C.F. Martín, *Sep. Purif. Technol.*, **276**, 119326 (2021); https://doi.org/10.1016/j.seppur.2021.119326
17. M. Clausse, J. Merel and F. Meunier, *Int. J. Greenh. Gas Control*, **5**, 1206 (2011); https://doi.org/10.1016/j.ijggc.2011.05.036
18. H. Vogtenhuber, R. Hofmann, F. Helminger and G. Schöny, *Energy*, **162**, 200 (2018); https://doi.org/10.1016/j.energy.2018.07.193
19. N. Jiang, Y. Shen, B. Liu, D. Zhang, Z. Tang, G. Li and and B. Fu, *J. CO2 Utiliz.*, **35**, 153 (2020); https://doi.org/10.1016/j.jcou.2019.09.012
20. M.P.S. Santos, C.A. Grande and A.E. Rodrigues, *Ind. Eng. Chem. Res.*, **50**, 974 (2011); https://doi.org/10.1021/ie100757u
21. S. Punpee and C. Phalakornkule, *Mater. Today Proc.*, **52**, 2517 (2021); https://doi.org/10.1016/j.matpr.2021.10.442
22. M.F.M. Post, in eds.: H. van Bekkum, E.M. Flanigen and J.C. Jansen, Diffusion in Zeolite Molecular Sieves, In: Introduction to Zeolite Science and Practice, Elsevier: Amsterdam, The Netherlands: Chap. 11, pp. 391-443 (1991).
23. D. M. Ruthven, Principles of Adsorption and Adsorption Processes, John Wiley & Sons, New York, NY, USA (1984).
24. E. Khoramzadeh, M. Mofarahi and C.-H. Lee, *J. Chem. Eng. Data*, **64**, 5648 (2019); https://doi.org/10.1021/acs.jced.9b00690
25. Y. Li, G. Yu and C. Wang, *Chin. J. Process Eng.*, **18**, 301 (2018); https://doi.org/10.12034/j.issn.1009-606X.217233
26. T. Montanari and G. Busca, *Vibr. Spectrosc.*, **46**, 45 (2008); https://doi.org/10.1016/j.vibspec.2007.09.001
27. Y. Shen, W. Shi, D. Zhang, P. Na and B. Fu, *J. CO2 Utiliz.*, **27**, 259 (2018); https://doi.org/10.1016/j.jcou.2018.08.001
28. N. Tlili, G. Grévillot and C. Vallières, *Int. J. Greenh. Gas Control*, **3**, 519 (2009); https://doi.org/10.1016/j.ijggc.2009.04.005
29. N. Jiang, Y.H. Shen, B. Liu, D.H. Zhang, Z.L. Tang, G.B. Li and B. Fu, *J. CO2 Util.*, **35**, 153 (2020); https://doi.org/10.1016/j.jcou.2019.09.012